



# Adsorption of Pb (II) ions from Aqueous Solution Using CuO-ZnO Nanocomposites

Sumon Chakrabarty<sup>1</sup> · Afrashim Tamim<sup>1</sup> · Murat Yilmaz<sup>2</sup> · Palash Kumar Dhar<sup>1</sup> · Rad Mosharrof Mim<sup>1</sup> · Sagar Kumar Dutta<sup>1</sup>

Received: 16 September 2022 / Accepted: 24 November 2022 / Published online: 7 December 2022  
© The Tunisian Chemical Society and Springer Nature Switzerland AG 2022

## Abstract

The present study aimed to synthesize Copper oxide-Zinc oxide nanocomposites (CuO-ZnO NCs) based on the sol-gel method, which was further used as a novel platform for the elimination of Pb (II) from aqueous solution. The crystallite structure, elemental composition, and surface morphology of the synthesized NCs were confirmed by utilizing different spectroscopic techniques. The obtained results revealed that the average size of CuO-ZnO NCs was 27.2 nm with a uniform distribution of spherical particles. According to batch experiments, the maximum removal percentage of Pb (II) ions (95.68%) was observed within 60 min at pH 5, adsorbate dose of 50 mg/L, and an adsorbent dose of 0.01 g. Isotherm modeling and kinetics studies showed that the adsorption of Pb (II) ions perfectly followed the Freundlich isotherm and pseudo-second-order kinetics. Overall, the CuO-ZnO NCs could be used as an effective adsorbent for the removal of Pb (II) ions from an aqueous solution due to their high adsorption capacity.

**Keywords** Heavy metals · Adsorption · Lead · Adsorption capacity · CuO-ZnO nanocomposites

## 1 Introduction

Recently, environmental issues about heavy metals have increased dramatically [1]. In societies where industrialization is developing, heavy metals such as the highly toxic lead (Pb) are discharged into natural rivers [2]. The main causes of lead (Pb) pollution are the release of industrial wastewater such as metallurgy, metal plating, and paper printing to the environment without treatment [3]. The concentration of lead in wastewater that exceeds the permissible levels can pose a serious threat to the environment, human health, and animals, leading to brain damage, behavioral problems, anemia, and mental disability [4]. Thus, lead (Pb) removal from surface waters or wastewaters is mandatory.

Today, numerous well-known techniques have been used extensively, such as chemical precipitation [5], membrane

filtration [6, 7], electrochemical separation [8, 9], coagulation [10], reverse osmosis [11, 12], ion exchange [13–15], solvent extraction [16], and adsorption [17] for ion removal. The adsorption technique has drawn much attention due to its low cost and simplicity [18–20]. Numerous types of adsorbents, such as plant wastes [21], activated carbon [22, 23], microorganisms [24], nano-graphite encapsulated alginate beads [25], fly ash [26], industrial and agricultural by-products [27], clay minerals [28] and carbon nanotubes [29] have been used for the sequestration of heavy metals from sewage.

Today, nanoparticles (NP)/nanocomposites (NC) developed with the development of nanotechnology are used as a good adsorbent in the removal of heavy metals and dyes [30, 31]. Nanocomposites (NC) are formed heterogeneously in multiple stages from multicomponent materials with at least one phase on the nanometer scale. The resulting NCs are used in a variety of applications such as the energy industry, food packaging, soil fertility improvement, wastewater treatment, and drug distribution [32, 33]. NCs have distinctive chemical properties, high surface areas, active functional groups, and high electron mobility in polyphase materials since at least one of their phases has a nanometer size [32]. As a result, nanocomposites illustrate better

✉ Sumon Chakrabarty  
sumonchakrabarty@ku.ac.bd

<sup>1</sup> Chemistry Discipline, Khulna University, 9208 Khulna, Bangladesh

<sup>2</sup> Department of Chemical Engineering, Faculty of Engineering, Osmaniye Korkut Ata University, 80000 Osmaniye, Turkey

selectivity, adsorption capacity, and stability against toxic pollutants than nanoparticles. These features can be developed in three different ways (i) by surface modification of the nanocomposites by some reagents like CTAB, SDS, etc. (ii) nanoparticles or nanocomposites loaded on biochar/graphene/activated carbon product, and (iii) by using graphene product/polymer material/biomass/chemicals in synthesis pathways [34–36].

Metal oxides are an extensively applied material for multiple industrial applications. Among numerous metal oxides, ZnO is known as a multifunctional material as it can be used in numerous fields such as electronics, converters, biomedicine, energy generator, optoelectronics, pro-ecological systems, or photocatalysts in hydrogen production and sensors [37, 38]. Among metal oxides, ZnO-based composites are one of the most preferred oxides and have wide applications in adsorption and photocatalysis [39, 40]. The ZnO is high mechanical and thermal stability at room temperature, high chemical stability, rigidity, hardness, and piezoelectric constant while its hybrid property is low toxicity, biodegradability, and biocompatibility [41]. In addition, the morphological, structural, electrical, and optical characteristics of the nanoscale ZnO can also be easily modified or enhanced for numerous applications [42]. ZnO-Tetrapod (ZnO-T) based nanocomposites synthesized by Sharma et al. showed high efficiency in the removal of heavy metal ions and organic dyes by adsorption and photocatalytic processes. Therefore, 3-dimensional nano- and micro-structured ZnO-Tetrapods (ZnO-T) show an important potential in adsorption/photocatalytic applications thanks to their large surface areas, high mechanical strength, high porosity and durability under harsh conditions [43, 44]. In addition, the study by Chowdhury et al. on the adsorption of organic dye and toxic metal ions using Ni – Co – S/ SDS composites gave good results [45]. We combine the bifunctional activity of ZnO and CuO nanoparticles to eliminate lead (Pb) (II) ions from the aqueous solution.

The sol–gel process is known to be widely utilized in ceramics engineering and materials science, where a colloidal solution (sol) is converted into an integrated network (gel) of network polymers or discrete particles [46]. By using this method, stable composites with high efficiency and performance can be synthesized under ambient conditions [47]. The nanoparticles used in these hybrids are: TiO<sub>2</sub> [48, 49], SiO<sub>2</sub> [50], Fe<sub>3</sub>O<sub>4</sub> [51], Al<sub>2</sub>O<sub>3</sub> [52], ZrO<sub>2</sub> [53], ZnO [54, 55] and CuO [54, 56, 57]. Numerous studies have been conducted on the production of nanocomposites by the sol–gel method. For instance, Wang et al. [58] prepared a Chitosan-silica composite for the removal of Congo red from wastewater. Wu et al. [59] studied the removal of cadmium (II) with a thiocyanate-functionalized silica gel they had prepared. In another study, mercaptopropyl coated cobalt ferrite (CoFe<sub>2</sub>O<sub>4</sub>) magnetic nanoparticles were prepared

by Viltuznik et al. [60] and utilized as an adsorbent in the elimination of Hg<sup>2+</sup> ions.

According to the literature research, ZnO/CuO composites, which were previously used in sensor construction [61, 62], hydrogen production [63] or photocatalytic studies [64, 65] were used for the first time in lead (Pb) removal by adsorption process in this study. This study is very important in order to see the synergistic effects of ZnO and CuO in the removal of Pb by the adsorption process. In addition, the high adsorption capacity (50 mg/g) of the obtained composites shows that it is more effective in lead (Pb) removal than other adsorbents in the literature.

In this study, copper oxide (CuO)-zinc oxide (ZnO) was produced by the sol–gel method and utilized as an adsorbent to eliminate lead (Pb) from wastewater. The physicochemical characteristics of the manufactured adsorbent were characterized by XRD, FTIR, SEM, and EDX analysis. The operating parameters comprising contact time, solution pH, adsorbate dosage, and the adsorbent dose were studied to understand the adsorption process, and also isothermal and kinetics parameters were determined.

## 2 Materials and Methods

### 2.1 Reagents and Instruments

In this experiment, analytical reagent-grade chemicals such as Lead nitrate, Zinc acetate, copper chloride, Ethanol, Citric acid, Hydrochloric acid, and Sodium hydroxide were purchased from Merck, India, and Loba Chemie, India, and used without any further pretreatment. For preparing the stock solution, deionized water (RCI Labscan, Thailand) was used. The metal pH and concentration in the studied samples were determined by using a pH meter (model HI96107, Hanna Instruments, USA) and atomic absorption spectrophotometer (AA-7000, Shimadzu), respectively. The surface morphology and elemental composition of synthesized NCs were investigated by relying on a Field emission scanning electron microscope (FESEM) coupled with an energy dispersive X-ray analyzer (EDS) (JEOL JSM-6390LA). To get an insight into the crystal structure of NCs, X-ray diffraction (XRD) instrument (Empyrean, PANalytical-Netherlands) was used. The presence of different functional groups on the surface of newly synthesized CuO-ZnO NCs was identified by Fourier Transform Infrared (FT-IR) Spectroscopy (Shimadzu IRAffinity-1, Japan).

### 2.2 Synthesis of CuO-ZnO Nanocomposites

The synthesis of CuO-ZnO NCs was carried out based on the well-known sol–gel method [66]. Initially, 25 mL of ethanol retaining 5.3247 g of zinc acetate, and 25 mL

of distilled water containing 6.3 g of citric acid were mixed in four separated beakers with vigorous stirring for an hour. Thereafter, 0.4244 g, 0.6741 g, 0.9488 g, and 1.2733 g of copper chloride were separately added to the above suspension at 60 °C with continuous stirring for 3 h. The final mixture containing beakers was kept in a dark place for 48 h. To avoid any kinds of contamination and interference of metallic impurities, the reagent mixtures were washed several times using deionized water. The obtained gel particles were dried at 120 °C and calcined at 500 °C for 4 h to get desired CuO-ZnO NCs.

### 2.3 Batch Adsorption Experiments

Initially, 1000 mg/L stock solution of Pb (II) ions was made from lead nitrate salt, which was obtained from the aforementioned suppliers. After that, the stock solution was further diluted to obtain various concentrations of Pb (II) solution for further studies. The pH of the solution was maintained by adding freshly prepared 0.1 M NaOH and 0.1 M HCl solution. The overall adsorption process of Pb (II) was performed in batch mode. To investigate the adsorption behavior of CuO-ZnO NCs, about 0.01 g of the synthesized NCs was taken into a reagent bottle containing 25 mL of experimental lead (II) solution, and the mixture was shaken at 160 rpm on a mechanical shaker at room temperature. The concentration of Pb (II) ions was determined using an atomic absorption spectrophotometer at a regular interval of time. The sequestration percentage of lead (II) ions (% R) and the adsorption efficacies ( $q_e$ ) of CuO-ZnO NCs (mg/g) can be estimated based on Eq. 1 and Eq. 2, respectively.

$$\%R = \frac{C_i - C_f}{C_i} \times 100 \quad (1)$$

$$q_e = \frac{C_i - C_f}{M} \times V \quad (2)$$

where,  $C_i$  and  $C_f$  indicated initial and final concentrations of lead (II) ions, respectively;  $V$  represented the volume of the metallic solution (L);  $M$  denoted the amount of dose of CuO-ZnO NCs (g).

### 2.4 Error Functions

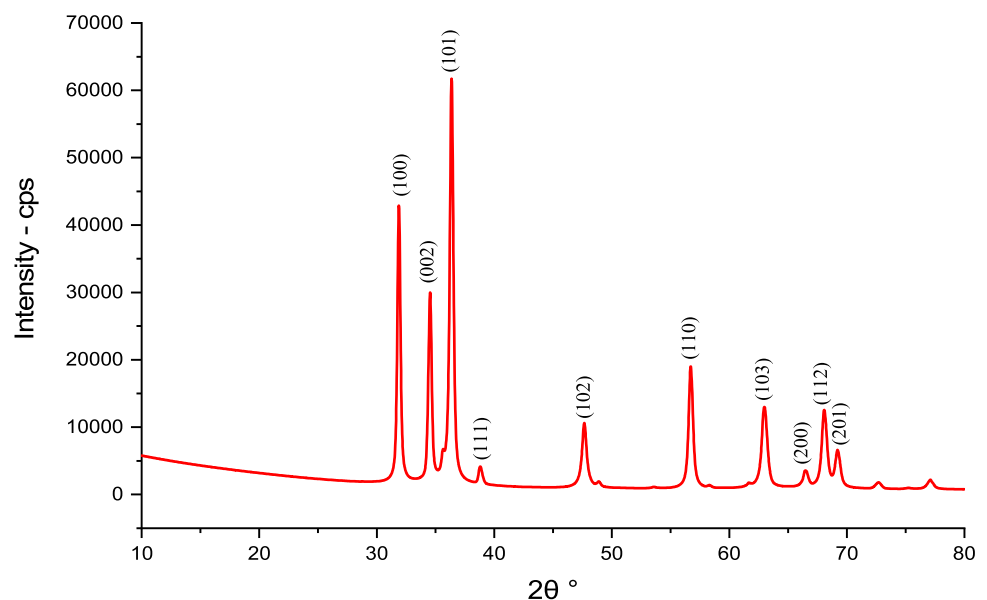
The error functions are an important statistical parameter used to measure the deviation of theoretically predicted isotherm parameters for evaluating the suitability of the isotherm and Kinetics model onto experimental results [67]. In this study, five different error functions include Residual Sum of Squares Error (ERRSQ/SSE), Chi-square ( $\chi^2$ ), Coefficient of determination ( $R^2$ ), Average Relative Error (ARE), Hybrid Fractional Error Function (HYBRID), Marquardt's Percent Standard Deviation (MPSD) were examined and in each case the isotherm and kinetics parameters were determined [67–69].

## 3 Results and Discussion

### 3.1 Characterization of Nanocomposites

Figure 1 shows the XRD pattern of CuO-ZnO NCs for different planes. The diffraction peaks ( $2\theta$ ) at 31.8°,

**Fig. 1** The XRD pattern of CuO-ZnO NCs.



34.5°, 36.3°, 47.6°, 56.6°, 62.9°, 66.4°, and 69.1° were corresponding to the crystal planes of (100), (002), (101), (110), (103), (112), (201), and (200), respectively. These XRD peaks fairly matched with the reported XRD data for ZnO particle (JCPDS card No. 01-075-9742) with a Wurtzite structure. Apart from these, a new diffraction peak was noticed at 38.7° which was indexed to the (111) for CuO [70]. The appearance of a new peak was probably due to the incorporation of CuO into ZnO. Therefore, the obtained results from the XRD pattern revealed the successful impregnation of CuO particles onto the surface of the ZnO matrix resulting in the formation of CuO-ZnO NCs.

The size of the CuO-ZnO NCs was calculated based on the Debye–Scherrer Eq. 3.

$$D = \frac{\rho\lambda}{\delta\cos\theta} \quad (3)$$

where,  $\delta$  represented the full width at half-maximum (FWHM) in radian,  $\theta$  indicated Bragg's angle in radian,  $\lambda$  denoted the wavelength of the incident X-rays,  $\rho$  is a constant (0.9), and  $D$  was the diameter of NCs [71]. The particle size at all crystal planes was separately calculated and the average crystallite size of CuO-ZnO NCs was estimated at  $\sim 27.2$  nm.

The FTIR spectrum of CuO-ZnO NCs is represented in Fig. 2. This spectrum exhibited a characteristic band in the 3000–3500  $\text{cm}^{-1}$  region, which indicated the presence of the O–H group. The band near 1550  $\text{cm}^{-1}$  was attributed to the carbonyl functional group (C=O), which possibly came due to the decomposition of ZnO from the precursor of  $\text{Zn}(\text{CH}_3\text{COO})_2 \cdot 2\text{H}_2\text{O}$ . The strong additional peak in the lower frequency range (500–700  $\text{cm}^{-1}$ ) ascertained the

stretching vibration of metal-oxygen, which might be due to the presence of ZnO and CuO in the synthesized ZnO-CuO NCs [72, 73].

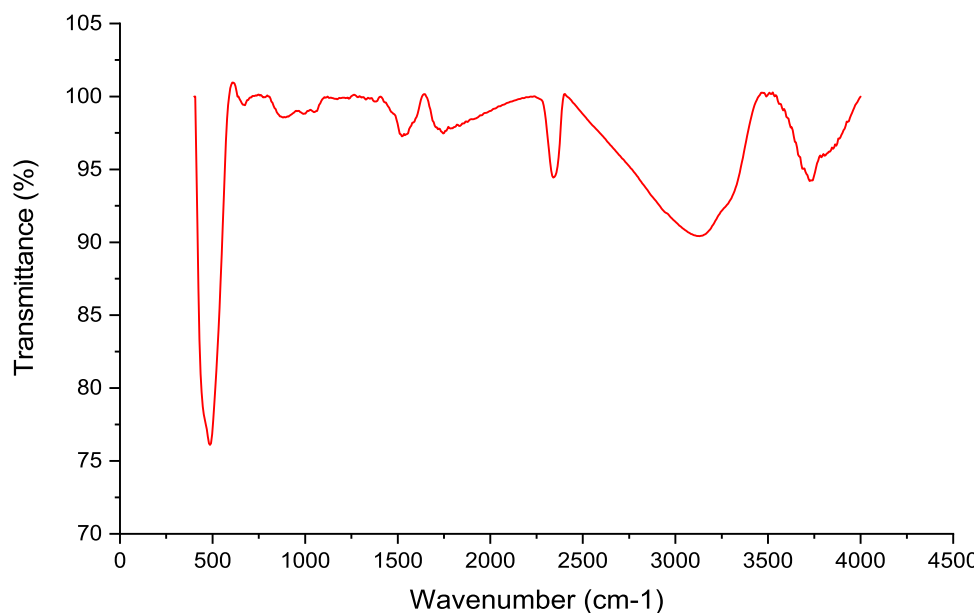
The detailed information regarding the structure and morphology of CuO-ZnO NCs was inspected by the FESEM and are shown in Fig. 3a, b. The surface morphology of CuO-ZnO NCs was uniform spherical. From these images, it was revealed that the size of synthesized NCs was in the nanometer range that supported the obtained result of XRD. The elemental composition of CuO-ZnO NCs is shown in Fig. 3e. The intense peak for Zinc (Zn), Copper (Cu), and Oxygen (O) was found in the EDS spectrum at different line-scanning values. Besides, the absence of other peaks within the detection limit indicated the purity of CuO-ZnO NCs, and the NCs were composed of Zn, Cu, and O elements only.

SEM analysis was also carried out to observe the morphology of the fabricated after the sorption of CuO-ZnO Nanocomposite (Fig. 3c, d). After adsorption the surface of the adsorbent remain as aggregates with the increasing of size. This might be due to the incorporation of the pb onto the nanocomposite surface. This observation was reconfirmed by EDX analysis after the sorption (Fig. 3f) which indicate the presence of pb atom as evidence of pb adsorption onto nanocomposite.

### 3.2 Effect of pH

The adsorption behavior of adsorbents is strongly influenced by the pH of the solution. Besides, the value of pH or the concentration of hydronium ions plays a pivotal role during the adsorption of heavy metals. The hydronium ion has a tendency to be adsorbed onto the

**Fig. 2** Infra-red (FTIR) spectra of CuO-ZnO NCs





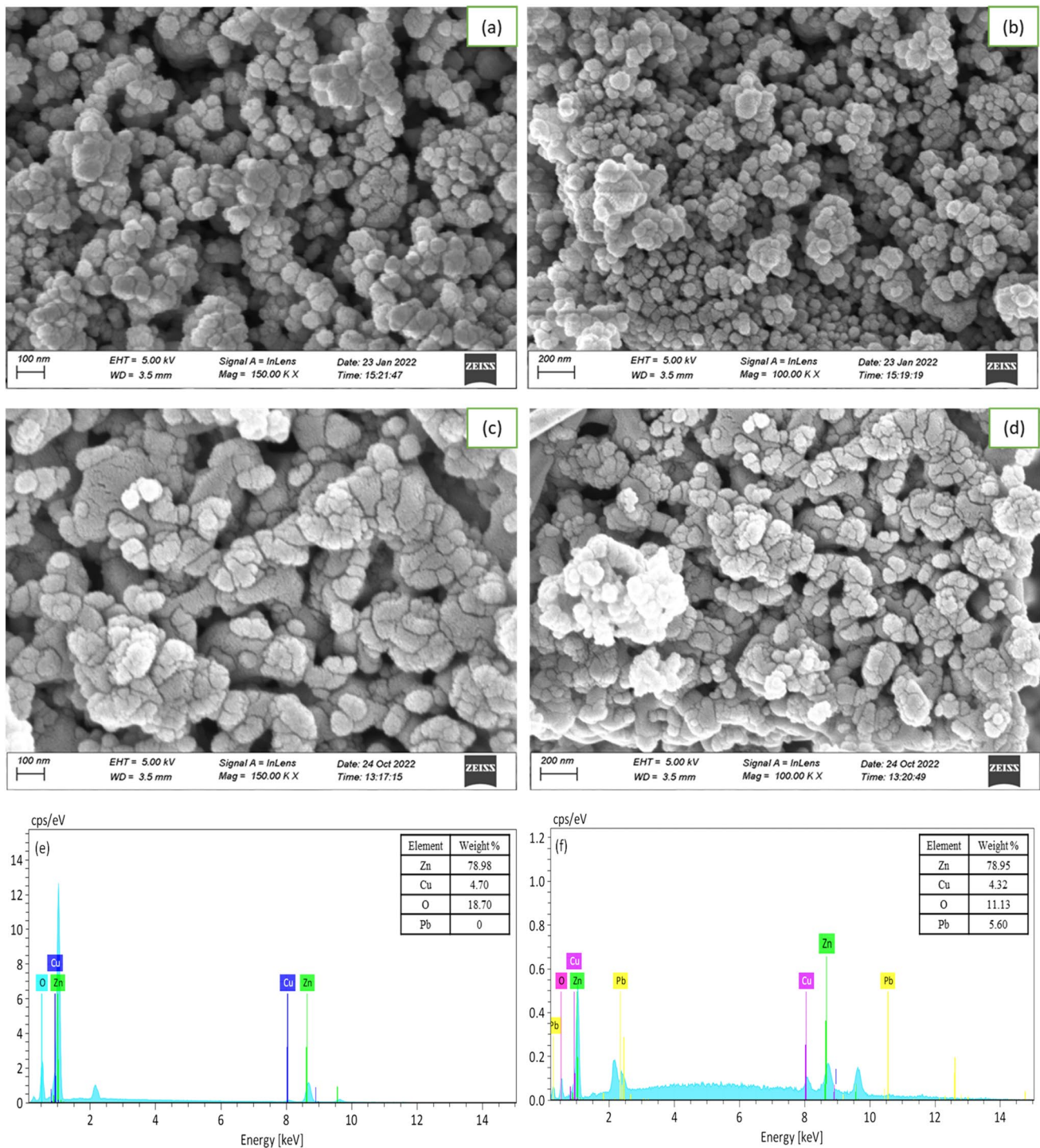


**Fig. 3** a, b FESEM image before adsorption. c, d FESEM image after adsorption. e EDS mapping before adsorption. f EDS mapping after adsorption of CuO-ZnO Nanocomposite

surface of NCs which arises a competition between the metal and hydronium ions. Such property of hydronium ion remarkably affects the adsorption capacity of the NCs towards the metal ions. To investigate the effect of pH on the adsorption behavior of NCs, the initial pH values of

the studied aqueous solution were adjusted from 2.0 to 7.0 by using freshly prepared 0.1 M HCl and 0.1 M NaOH solution. In this study, the batch experiments over pH 7 were not carried out because the precipitation of metal

complexes occurs that hindered the heavy metal removal process [74].

While screening the optimum pH value, all the other variables such as initial concentration of Pb (II) ions ( $50 \text{ mg L}^{-1}$ ), adsorbent dose ( $0.01 \text{ mg}/25 \text{ mL}$ ), and contact time (1 h) were kept constant. From Fig. 4a, it can be seen that the elimination percentages of Pb (II) ions from an aqueous system by the CuO-ZnO NCs adsorbents varied at different pHs. The removal of Pb (II) ions sharply increased up to pH 5 where the highest removal (95.68%) of Pb (II) ions was observed. After this point, the removal percentage gradually decreased. At lower pH, the active sites of the adsorbents became protonated due to the greater availability of protons, hence, the adsorption capacity of adsorbents was reduced [75]. On the other hand, increasing the pH values after pH 5, the adsorption percentage also decreased possibly due to the formation of hydroxyl complexes such as  $\text{Pb}(\text{OH})_2$ ,  $\text{PbOH}^+$ , aqueous  $\text{Pb}(\text{OH})_2$ , and  $\text{Pb}(\text{OH})_3^{3-}$  [76–79].

### 3.3 Effect of Contact Time

The contact time between the Pb (II) ions and CuO-ZnO NCs has a significant influence in batch adsorption studies.

In this experiment, the removal percentages of Pb (II) ions ( $50 \text{ mg/L}$ ) were monitored at room temperature, optimum pH 5, and different contact times (15, 30, 45, 60, 75, and 90 min). Figure 4b showed that the adsorption of metal ions dramatically increased to attain optimum contact time, and after 60 min a downward trend was noticed. This phenomenon indicated the surface of the CuO-ZnO NCs was saturated with the Pb (II) ions so that it experienced desorption or the metal ions being released into solution because there was insufficient active site capable of binding to Pb (II) metal ions on the surface of the adsorbent [80].

### 3.4 Effect of Concentration

The initial concentration of metal ions in an aqueous solution controls the metal ion adsorption. The effect of Pb (II) ions concentration on removal percentages was investigated by varying the metal ion concentration from 10 to 60 mg/L by keeping other parameters constant (contact time 1 h, optimum pH 5, dose  $0.01 \text{ g}$ ). Figure 4c showed that increasing the initial concentration of Pb (II) ions enhances the removal percentage, which was similar to the previously reported findings [81, 82]. This phenomenon can be explained by the fact that improving the specific area of

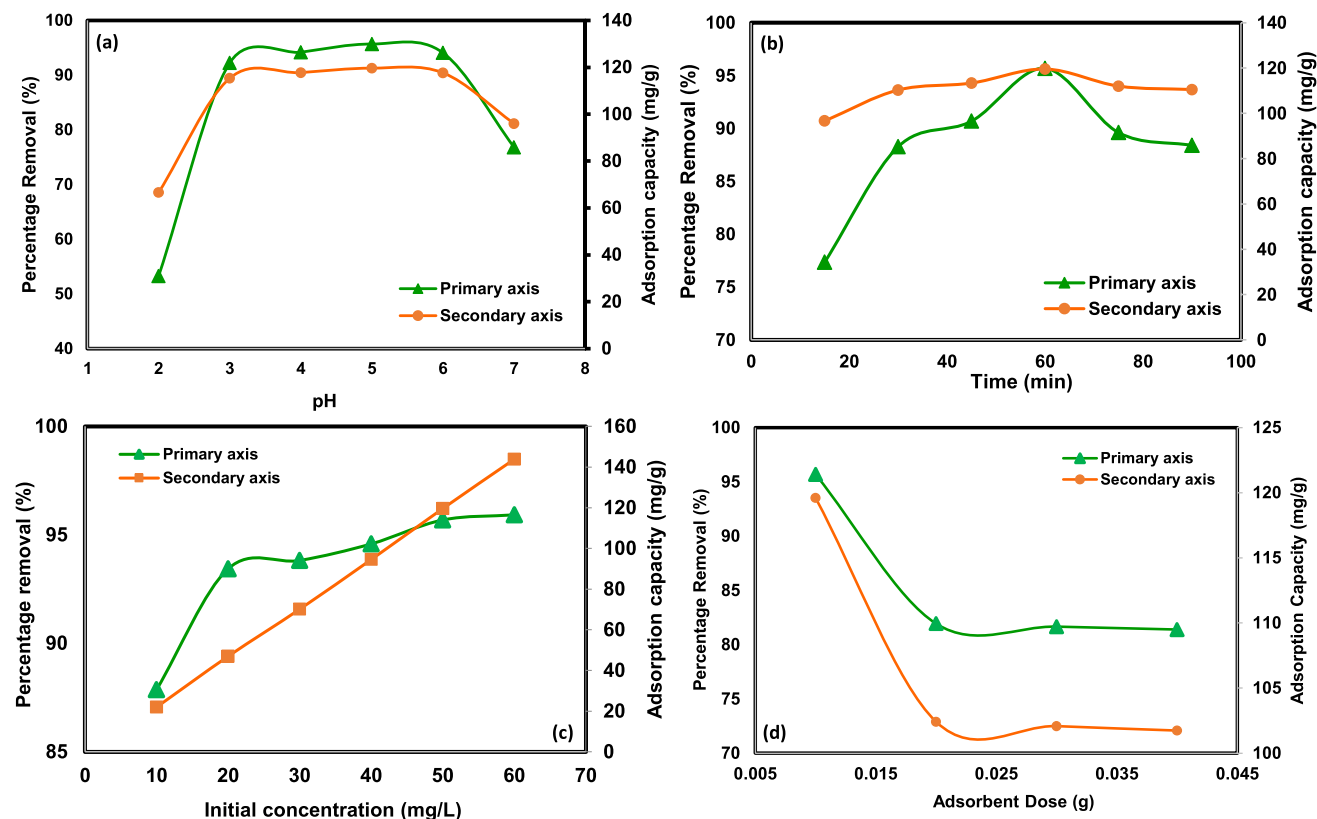


**Fig. 4** a Influence of pH. b Influence of contact time. c Influence of initial concentration of metal ions. d Influence of adsorbent dose on the removal percentage of Pb (II) ions using *CuO-ZnO Nanocomposites*

the adsorbent increases the possibility of collision between the metal ions and adsorbent particles [83].

### 3.5 Effect of CuO-ZnO NCs Dose

The effect of the adsorbent dose on the removal percentage of Pb (II) ions was performed by adding different amounts of CuO-ZnO NCs (0.01 to 0.04 g) having initial concentration of Pb (II) ions (50 mg/L), contact time 1 h and optimum pH 5. From Fig. 4d it can be noticed that by increasing the concentration of CuO-ZnO NCs the removal percentage was decreased and after the addition of 0.02 to 0.04 g of adsorbents, the removal of Pb (II) ion remained almost constant. At lower concentrations, greater removal of Pb (II) ions was observed, which was possibly due to the large surface area of adsorbents or the availability of exchangeable active sites of CuO-ZnO NCs on which the metal ions can get adsorbed [76]. Contrarily, by increasing the dose of NCs, the total number of active sites on the adsorbents gradually increases, thus the aggregation or overlapping of active sites occurs which significantly reduces the sequestration percentage of Pb (II) ions [84].

### 3.6 Equilibrium Studies and Isotherm Modeling

For equilibrium and isothermal modeling studies, the well-known Freundlich and Langmuir equations were used.

These equations generally describe the co-relation between equilibrium metal biosorption and final concentrations at equilibrium. Langmuir’s equation was derived based on the principle that the maximum sorption occurs corresponding to the saturated monolayer formation of sorbate ions on the adsorbent surface. On the other hand, the Freundlich isotherm equation is basically used to determine the adsorption capacity of the sorbent toward the adsorbents. The Langmuir and Freundlich equations were expressed by the Eqs. 4 and 5 [85, 86].

$$\frac{C_e}{Q_e} = \frac{C_e}{Q_m} + \frac{1}{bQ_m} \tag{4}$$

$$\log Q_e = \log K_f + \frac{1}{n} \log C_e \tag{5}$$

where,  $Q_m$ ,  $b$ ,  $C_e$ ,  $Q_e$ ,  $K_f$ , and  $n$  indicated the Langmuir constant, adsorption energy, the equilibrium concentration of Pb (II) (in mg/L), the amount of metal adsorbed per unit weight of adsorbent (in mg/g), the relative adsorption capacity of CuO-ZnO NCs, and the deviation for the adsorption system, respectively.

The adsorption isotherm curves were constructed based on the Langmuir and Freundlich models, which are depicted in Fig. 5a, b. The calculated value of Langmuir’s and Freundlich’s constants are represented in Table 1. The linear plots

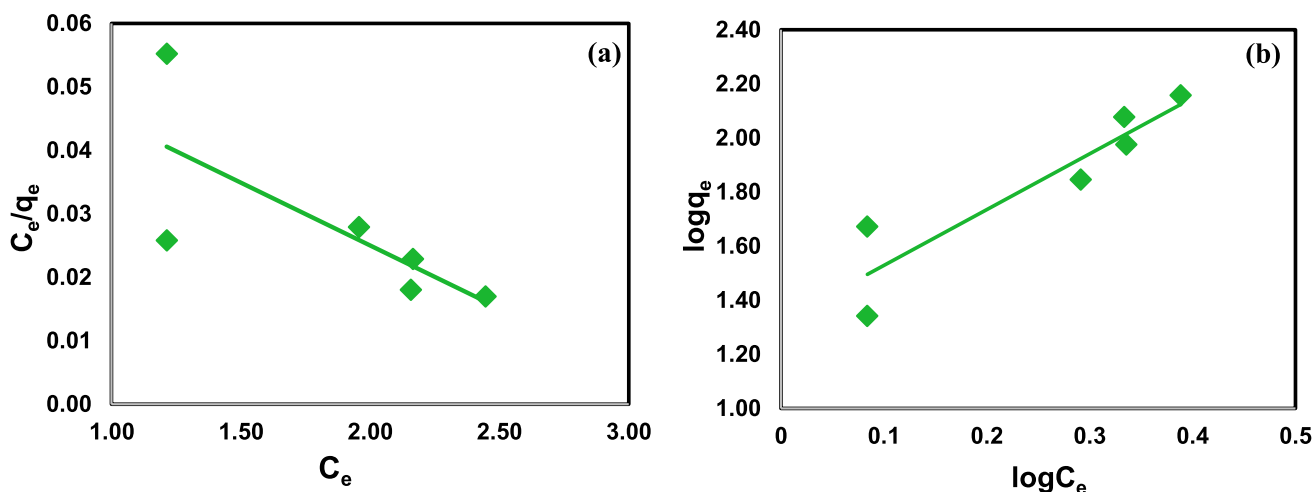


Fig. 5 The linear plots of **a** the Langmuir and **b** the Freundlich adsorption isotherm model

**Table 1** Parameter values of the isotherms adsorption of Pb (II) ion onto CuO-ZnO nanocomposite

Metal	Adsorbent	Langmuir constant			Freundlich constant	
		1/b	$Q_{max}$ (mg/g) (cal.)	$Q_{max}$ (mg/g) (expt.)	k	n
Pb <sup>2+</sup>	CuO-ZnO Nanocomposites	3.2679	50.50	119.60	21.0474	0.4847

of isotherm modeling showed that the Freundlich isotherm was best fitted for explaining the adsorption of Pb (II) ions onto the surface of CuO-ZnO NCs. The  $R^2$  value of the Freundlich isotherm was 0.852, which was close to unity (1.0) as compared to the value of Langmuir's constant (0.5431). This finding revealed that Pb (II) ions were adsorbed on the uneven surface by multilayer formation and there was an uneven energy distribution among the surface-active sites of the NCs [87].

However, the degree of nonlinearity between adsorbents and the concentrations of metal ion solution is denoted by the symbol “ $n$ ”. Depending on the value of  $n$ , the adsorption process can be classified into three categories such as (i) chemical (ii) physical, and (iii) linear adsorption process. For explaining physical, chemical, and linear processes, the value of  $n$  should be  $n > 1$ ,  $n < 1$ , and  $n = 1$ , respectively. In this study, the value of  $n$  in Freundlich isotherms was observed less than one, which revealed the removal of Pb (II) ions by CuO-ZnO NCs proceeded via the chemical adsorption. It is noteworthy that the value of  $1/n$  was observed greater than 1.0, which indicates co-operative process between the adsorbate-adsorbent interactions [88]. However, the maximum adsorption capacity ( $q_m$ ) was found to be 50.50 mg/g, which was obtained from Langmuir's model.

### 3.7 Adsorption Kinetics

The adsorption phenomenon between adsorbates and adsorbents could be explained by chemical reactions, diffusion control, mass transfer, and particle diffusion mechanisms. For well understanding of the adsorption process, Lagergren's pseudo-first-order, and pseudo-second-order kinetic models were considered and fitted with the experimental data by using Eq. 6 and Eq. 7, respectively.

These models have a pivotal role in explaining the adsorption behavior of liquid or solid systems [89].

$$(\ln q_e - \ln q_t) = \ln q_e - K_1 t \quad (6)$$

$$\frac{t}{q_t} = \frac{t}{q_e} + \frac{1}{K_2 q_e^2} \quad (7)$$

where  $q_e$  and  $q_t$  indicated the amounts (mg/g) of Pb (II) ions adsorbed at equilibrium and at time  $t$  (min), respectively;  $k_1$  ( $\text{min}^{-1}$ ) and  $k_2$  (g/mg.min) denoted the rate coefficients for the pseudo-first-order and pseudo-second-order kinetic model, respectively. The value of  $k_1$  and  $q_e$  was calculated from the slope and intercept of the linear plot of  $\ln(q_e - q_t)$  vs.  $t$ , whereas, the value of  $q_e$  and  $k_2$  was obtained from the plot of  $t/q_t$  against  $t$ , as presented in Fig. 6a, b, respectively [90].

The value of kinetic parameters and coefficient of correlation ( $R^2$ ) for the pseudo-first-order and pseudo-second-order kinetic models are summarized in Table 2. The value of  $R^2$  for the pseudo-first-order reaction model (0.330) was much lower than that of the pseudo-second-order kinetic model (0.994), which was very close to 1.00. This finding revealed that the adsorption of Pb (II) ions by CuO-ZnO NCs in an

**Table 2** Parameter values of the kinetic studies of the adsorption of Pb (II) ion onto CuO-ZnO NCs

	Metal	$q_e$ (mg/g) (cal.)	$q_e$ (mg/g) (expt.)	$R^2$	$k$
Pseudo-first order kinetics	Pb	15.73	119.60	0.330	0.0092
Pseudo-second order kinetics		113.63	119.60	0.994	0.0087

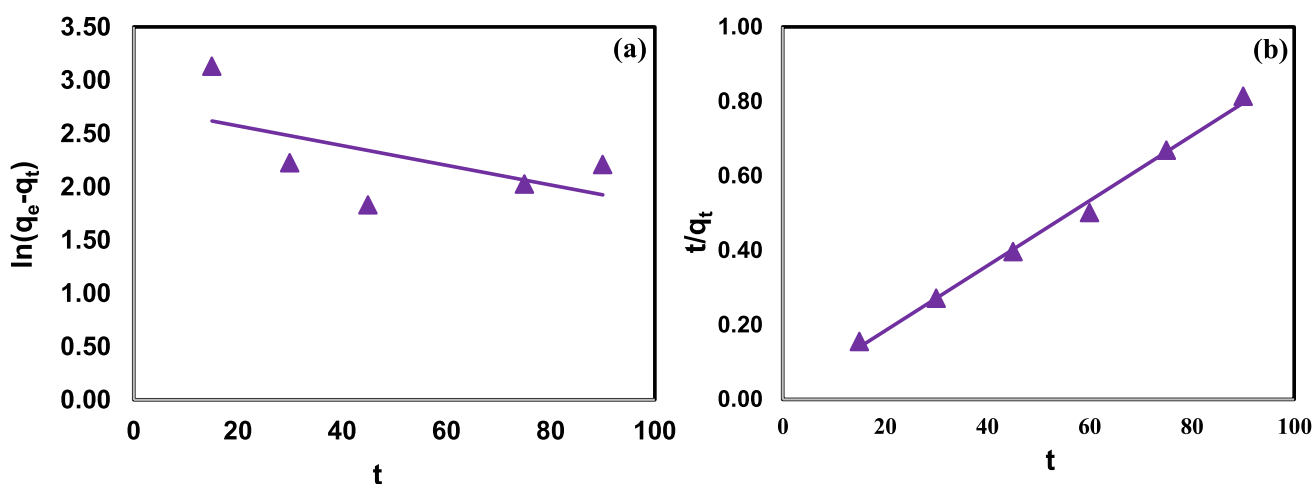


**Fig. 6** The linear plots, **a** pseudo-first-order and **b** pseudo-second-order kinetic models for the adsorption of Pb (II) ions onto CuO-ZnO NCs.



aqueous solution solely followed the pseudo-second-order kinetics. Besides, the difference between  $q_e$  (experiment.) and  $q_e$  (calculated) was less, which indicated that the adsorption process of Pb (II) ions onto the surface of CuO-ZnO NCs took place via the chemical interaction. The findings of our study comply with the previously published similar articles related to the adsorption of  $Pb^{2+}$  ions from aqueous solutions by different adsorbents [74, 91, 92].

Numerous researchers have developed different types of nanomaterials for studying the adsorption of Pb (II) ions from an aqueous solution. The findings of the present study showed that CuO-ZnO NCs have comparatively better performance in the elimination of Pb (II) ions than the previously reported adsorbents as given in Table 3.

### 3.8 Error Functions

In this study, the best-fitting isotherm was selected based on the error functions, which had the lowest error distribution between the experimental and predicted isotherms [67, 68].

The obtained results for the optimization of Freundlich and Langmuir isotherms by error function analysis are presented in Table 4. A comparison between the isotherm parameters showed that the Freundlich isotherm fitted the experimental sorption data much better than that of the Langmuir model as its  $R^2$ -value was higher than those for the respective ion for the Langmuir isotherm. On the other hand, the values of ARE, Hybrid,  $\chi^2$  and MPSD for the Freundlich model were comparatively lower than those of the Langmuir model [67, 69].

However, the error function analysis was also performed for two kinetic models and the obtained results are summarized in Table 5. From this table it can be seen that the  $R^2$ -value for pseudo-second-order kinetic (0.9941) was much higher than that of pseudo-first-order kinetic (0.4236). In addition to this, analysis of five error functions for the two kinetic models revealed that uptake of Pb(II) ion onto the surface of CuO-ZnO NCs was mostly favored by the pseudo-second-order kinetic model having comparatively lower RSS, ARE, Hybrid, Chi-square ( $\chi^2$ ) and MPSD values.

**Table 3** Comparison of efficacy of CuO-ZnO NCs with other similar studies

Adsorbent	pH	Contact Time (min)	Adsorption Capacity (mg/g)	Kinetics	Isotherm	Refs
Iron oxide nanoparticles	5.5	30	36.00	–	Langmuir Freundlich	[93]
magnesium oxide nanoparticles	9	280	16.44	–	Langmuir Freundlich	[94]
(ZnO) nanoparticle	4	–	26.11	–	Langmuir Freundlich	[95]
SiOH	3.7–8.5		46.30	Pseudo second order	-	[96]
CuO nanoparticle	6	120–180	14.20	Pseudo second order	Freundlich	[97]
Al <sub>2</sub> O <sub>3</sub> nanoparticle	5	20	47.08	–	Freundlich	[98]
crosslinked Chitosan-clay beads	4.5	80	7.93	–	Langmuir	[99]
Anatase Nanoparticles	6	750	31.25	Pseudo second order	Langmuir	[100]
CuO-ZnO nanocomposites	6	60 min.	50.00	Pseudo second order	Freundlich	This work

**Table 4** Error functions for optimization of equilibrium isotherms

Error functions	$R^2$	ERRSQ/ RSS	ARE	HYBRID	Chi-square ( $\chi^2$ )	MPSD
Freundlich Isotherm	0.8498	88.16706	-7.1243	-10.6865	3.01	33.2372
Langmuir Isotherm	0.5431	68.75373	6.2913	9.436962	3.12	70.8844

**Table 5** Error functions for optimization of adsorption kinetics

Error functions	$R^2$	ERRSQ/ RSS	ARE	HYBRID	Chi-square ( $\chi^2$ )	MPSD
Pseudo-first-order kinetic	0.4236	4951.26	12.1296	18.19449	51.21	52.9663
Pseudo-second-order kinetic	0.9941	50.4115	1.2239	1.83589	0.5214	3.3559

### 3.9 Thermodynamics Studies

Temperature is a major consideration in many adsorption processes, thus studying its thermodynamics is essential. Adsorption-related energy changes were quantified by altering the equilibrium constants with temperature and calculating the Gibbs free energy ( $\Delta G^\circ$ ), enthalpy ( $\Delta H^\circ$ ), and entropy ( $\Delta S^\circ$ ). The formula for determining the  $K_d$  distribution coefficient is given by Eq. 8, which is followed by Eq. 9 [101]

$$\Delta G = -RT \ln K_d \quad (8)$$

where,  $R$  is the universal gas constant ( $8.314 \text{ J mol}^{-1} \text{ K}^{-1}$ ),  $T$  is the temperature (K)

$$K_d = \frac{q_e}{C_e} \quad (9)$$

where,  $q_e$  and  $C_e$  are the equilibrium concentration of Pb (II) on ZnO-CuO ( $\text{mg L}^{-1}$ ) and in the solution ( $\text{mg L}^{-1}$ ), respectively. The following equations can also be written using  $\Delta G$ ,  $\Delta H$ , and  $\Delta S$  as the variables in the relationship [102].

$$\Delta G = \Delta H - T\Delta S \quad (10)$$

$$\ln K_d = \frac{\Delta S}{R} - \frac{\Delta H}{RT} \quad (11)$$

In a straight line plot of  $\ln K_d$  vs.  $1/T$ , both  $\Delta H$  and  $\Delta S$  may be determined from the slope and the intersection. Values for  $\Delta G$ ,  $\Delta H$ , and  $\Delta S$  were determined and are shown in Table 6. Figure 7 illustrates a plot of  $\ln K_d$  vs.  $1/T$  for Pb (II) adsorption on ZnO-CuO. Furthermore, the high enthalpy values ( $\Delta H > 20 \text{ kJ mol}^{-1}$ ) suggest that chemisorption plays a role in the adsorption process through an ion exchange mechanism. The adsorption process introduces an excessive amount of randomness at the solid-liquid interface, which is reflected by the positive values for entropy [101, 103]. The fact that the Gibbs energy has negative values suggests that the process is spontaneous, and the fact that these values are increasing suggests that the spontaneity is growing as the temperature rises [102–104].

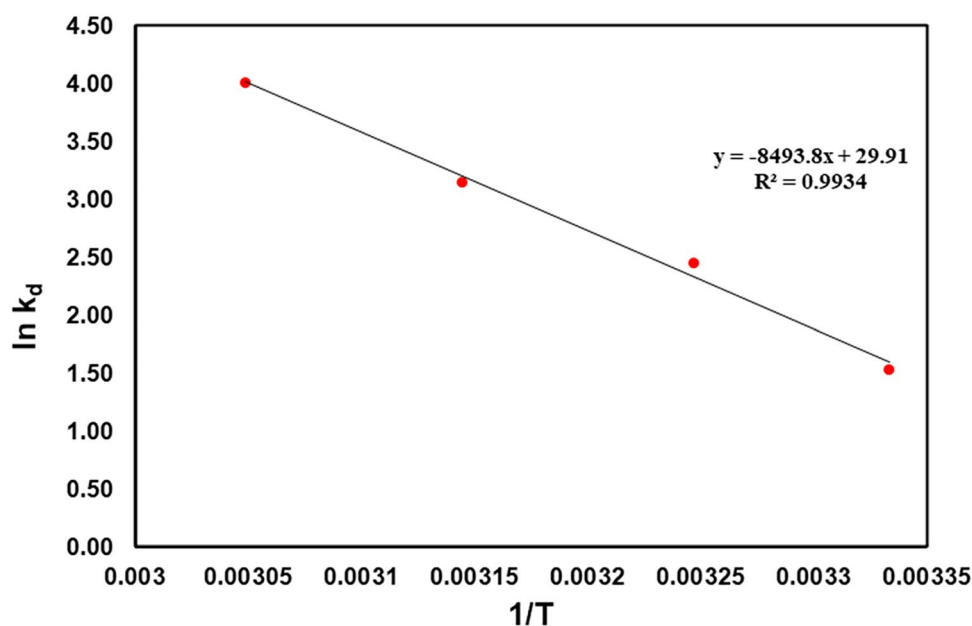
**Table 6** Thermodynamic parameters for Pb (II) removal by ZnO-CuO

Temperature (K)	$\Delta G$ ( $\text{kJ mol}^{-1}$ )	$\Delta H$ ( $\text{kJ mol}^{-1}$ )	$\Delta S$ ( $\text{J mol}^{-1} \text{ K}^{-1}$ )
300	-3.813	70.617	248.671
308	-6.283		
318	-8.326		
328	-10.935		

### 4 Conclusion

Safe drinking water is essential for maintaining sound health. In this current study, CuO-ZnO NCs were synthesized and characterized by using XRD, FTIR, FESEM, and EDX spectroscopic techniques, which were successfully used as an adsorbent for the removal of Pb (II) ions from aqueous solution. Batch adsorption experiments revealed that a

**Fig. 7**  $\ln K_d$  versus  $1/T$  graph for the determination of thermodynamic parameters for Pb (II) on adsorption on ZnO-CuO.



maximum of 95.68% removal were observed within one hour which was comparatively better than other similar studies. Therefore, the newly synthesized CuO-ZnO NCs could be used as a novel platform for the sequestration of Pb (II) ions from an aqueous solution.

**Acknowledgements** The study was financially supported by the research cell, Khulna University, Khulna-9208 Bangladesh through a research grant.

**Data Availability** Not applicable.

**Code Availability** Not applicable.

## Declarations

**Conflict of Interest** The authors declare no conflict of interest.

## References

- Burakov AE, Galunin EV, Burakova IV, Kucherova AE, Agarwal S, Tkachev AG (2018) Adsorption of heavy metals on conventional and nanostructured materials for wastewater treatment purposes: a review. *Ecotoxicol Environ Saf* 148:702–712. <https://doi.org/10.1016/j.ecoenv.2017.11.034>
- Habila MA, Alothman ZA, Yilmaz E, Soylak M (2018) Activated carbon cloth filled pipette tip for solid phase extraction of nickel(II), lead(II), cadmium(II), copper(II) and cobalt(II) as 1,3,4-thiadiazole-2,5-dithiol chelates for ultra-trace detection by FAAS. *Int J Environ and Ch* 98(2):171–181. <https://doi.org/10.1080/03067319.2018.1430794>
- Gupta VK, Rastogi A (2008) Biosorption of lead from aqueous solutions by green algae *Spirogyra* species: kinetics and equilibrium studies. *J Hazard Mater* 152(1):407–414. <https://doi.org/10.1016/j.jhazmat.2007.07.028>
- Wu X, Cobbina SJ, Mao G, Xu H, Zhang Z, Yang L (2016) A review of toxicity and mechanisms of individual and mixtures of heavy metals in the environment. *Environ Sci Pollut Res Int* 23(9):8244–8259. <https://doi.org/10.1007/s11356-016-6333-x>
- Wang Q, Gao W, Liu Y, Yuan J, Xu Z, Zeng Q (2014) Simultaneous adsorption of Cu(II) and SO<sub>4</sub><sup>2-</sup> ions by a novel silica gel functionalized with a ditopic zwitterionic Schiff base ligand. *Chem Eng J* 250:55–65. <https://doi.org/10.1016/j.cej.2014.03.106>
- Khulbe KC, Matsuura T (2018) Removal of heavy metals and pollutants by membrane adsorption techniques. *Appl Water Sci* 8(1). <https://doi.org/10.1007/s13201-018-0661-6>
- Borbély G, Nagy E (2009) Removal of zinc and nickel ions by complexation–membrane filtration process from industrial wastewater. *Desalination* 240(1–3):218–226. <https://doi.org/10.1016/j.desal.2007.11.073>
- Khatab IA, Shaffei MF, Shaaban NA, Hussein HS, Abd El-Rehim SS (2013) Electrochemical removal of copper ions from dilute solutions using packed bed electrode. Part II. *Egypt J Pet* 22(1):205–210. <https://doi.org/10.1016/j.ejpe.2012.09.012>
- Karami H (2013) Heavy metal removal from water by magnetite nanorods. *Chem Eng J*. <https://doi.org/10.1016/j.cej.2013.01.022>. 219:209–16
- Tang X, Zheng H, Teng H, Sun Y, Guo J, Xie W (2014) Chemical coagulation process for the removal of heavy metals from water: a review. *Desalin Water Treat* 57(4):1733–1748. <https://doi.org/10.1080/19443994.2014.977959>
- Yoon J, Amy G, Chung J, Sohn J, Yoon Y (2009) Removal of toxic ions (chromate, arsenate, and perchlorate) using reverse osmosis, nanofiltration and ultrafiltration membranes. *Chemosphere* 77(2):228–235. <https://doi.org/10.1016/j.chemosphere.2009.07.028>
- Qdaisa HA, Moussa H (2004) Removal of heavy metals from wastewater by membrane processes: a comparative study. *Desalination* 164:105–110. [https://doi.org/10.1016/S0011-9164\(04\)00169-9](https://doi.org/10.1016/S0011-9164(04)00169-9)
- Bashir A, Malik LA, Ahad S, Manzoor T, Bhat MA, Dar GN (2018) Removal of heavy metal ions from aqueous system by ion-exchange and biosorption methods. *Environ Chem Lett* 17(2):729–754. <https://doi.org/10.1007/s10311-018-00828-y>
- Anirudhan TS, Divya L, Ramachandran M (2008) Mercury (II) removal from aqueous solutions and wastewaters using a novel cation exchanger derived from coconut coir pith and its recovery. *J Hazard Mater* 157(2–3):620–627. <https://doi.org/10.1016/j.jhazmat.2008.01.030>
- Yuan P, Liu D, Fan M, Yang D, Zhu R, Ge F (2010) Removal of hexavalent chromium [Cr(VI)] from aqueous solutions by the diatomite-supported/unsupported magnetite nanoparticles. *J Hazard Mater* 173(1–3):614–621. <https://doi.org/10.1016/j.jhazmat.2009.08.129>
- Li Z, Wei Q, Yuan R, Zhou X, Liu H, Shan H (2007) A new room temperature ionic liquid 1-butyl-3-trimethylsilylimidazolium hexafluorophosphate as a solvent for extraction and preconcentration of mercury with determination by cold vapor atomic absorption spectrometry. *Talanta* 71(1):68–72. <https://doi.org/10.1016/j.talanta.2006.03.023>
- Chiban M, Soudani A, Sinan F, Persin M (2011) Single, binary and multi-component adsorption of some anions and heavy metals on environmentally friendly *Carpobrotus edulis* plant. *Colloids Surf B Biointerfaces* 82(2):267–276. <https://doi.org/10.1016/j.colsurfb.2010.09.013>
- Fall B, Gaye C, Niang M, Alli YA, Diaw AK, Fall M, Thomas S, Randriamahazaka H (2022) Removal of toxic chromium ions in Aqueous Medium using a New Sorbent based on rGO@CNT@Fe<sub>2</sub>O<sub>3</sub>. *Chem Afr* 17:1–3. <https://doi.org/10.1007/s42250-022-00499-x>
- Biswal SS, Panda C, Parida SR, Mallick SK, Jena T, Sahoo JK, Sahu D (2022) Removal of Hexavalent Chromium from Industrial Wastewater using Adsorbent prepared from Biomass IPO-MOEA CARNEA. *Chem Afr* 28:1–3. <https://doi.org/10.1007/s42250-022-00472-8>
- Bassam R, El Alouani M, Maissara J, Rachdi Y, El Khattabi EH, Saufi H, El Mahi Chbihi M, Belaouad S (2022) Nature and mechanism of the metals ions adsorption from a ternary aqueous medium using natural sedimentary rock. *Chem Afr* 16:1–6. <https://doi.org/10.1007/s42250-022-00424-2>
- Khan MA, Ngabura M, Choong TS, Masood H, Chuah LA (2012) Biosorption and desorption of Nickel on oil cake: batch and column studies. *Bioresour Technol* 103(1):35–42. <https://doi.org/10.1016/j.biortech.2011.09.065>
- Song S-T, Saman N, Johari K, Mat H (2013) Removal of hg(II) from aqueous solution by Adsorption using raw and chemically modified Rice Straw as Novel Adsorbents. *Ind Eng Chem Res* 52(36):13092–13101. <https://doi.org/10.1021/ie400605a>
- Ni Y, Jin L, Zhang L, Hong J (2010) Honeycomb-like Ni@C composite nanostructures: synthesis, properties and applications in the detection of glucose and the removal of heavy-metal ions. *J Mater Chem* 20(31). <https://doi.org/10.1039/c0jm00142b>
- Sari A, Tuzen M (2009) Removal of mercury(II) from aqueous solution using moss (*Drepanocladus revolvens*) biomass: equilibrium, thermodynamic and kinetic studies. *J Hazard Mater*

- 171(1–3):500–507. <https://doi.org/10.1016/j.jhazmat.2009.06.023>
25. Khan MA, Jung W, Kwon O-H, Jung YM, Paeng K-J, Cho S-Y (2014) Sorption studies of manganese and cobalt from aqueous phase onto alginate beads and nano-graphite encapsulated alginate beads. *J Ind Eng Chem* 20(6):4353–4362. <https://doi.org/10.1016/j.jiec.2014.01.043>
  26. He K, Chen Y, Tang Z, Hu Y (2016) Removal of heavy metal ions from aqueous solution by zeolite synthesized from fly ash. *Environ Sci Pollut Res Int* 23(3):2778–2788. <https://doi.org/10.1007/s11356-015-5422-6>
  27. Ahmaruzzaman M, Gupta VK (2011) Rice Husk and its Ash as low-cost adsorbents in Water and Wastewater Treatment. *Ind Eng Chem Res* 50(24):13589–13613. <https://doi.org/10.1021/ie201477c>
  28. Javadian H, Taghavi M (2014) Application of novel Polypyrrole/thiol-functionalized zeolite Beta/MCM-41 type mesoporous silica nanocomposite for adsorption of Hg<sup>2+</sup> from aqueous solution and industrial wastewater: kinetic, isotherm and thermodynamic studies. *Appl Surf Sci* 289:487–494. <https://doi.org/10.1016/j.apsusc.2013.11.020>
  29. Singh JK, Anitha K, Namsani S (2015) Removal of heavy metal ions using Functionalized single-walled Carbon Nanotube: a Molecular Dynamics Study. *ACS Paragon Plus Environment The Journal of Physical Chemistry*. <https://doi.org/10.1021/acs.jpca.5b03352>
  30. Afroze S, Sen TK (2018) A review on Heavy Metal Ions and Dye Adsorption from Water by Agricultural Solid Waste Adsorbents. *Water Air Soil Pollut* 229(7). <https://doi.org/10.1007/s11270-018-3869-z>
  31. Cheriyaundath S, Vavilala SL (2020) Nanotechnology-based wastewater treatment. *Water Environ J* 35(1):123–132. <https://doi.org/10.1111/wej.12610>
  32. Omanović-Miklićanin E, Badnjević A, Kazlagic A, Hajlovac M (2019) Nanocomposites: a brief review. *Health Technol* 10(1):51–59. <https://doi.org/10.1007/s12553-019-00380-x>
  33. Kabiri K, Omidian H, Zohuriaan-Mehr MJ, Doroudiani S (2011) Superabsorbent hydrogel composites and nanocomposites: a review. *Polym Compos* 32(2):277–289. <https://doi.org/10.1002/pc.21046>
  34. Chen H, Wageh S, Al-Ghamdi AA, Wang H, Yu J, Jiang C (2019) Hierarchical C/NiO-ZnO nanocomposite fibers with enhanced adsorption capacity for Congo red. *J Colloid Interface Sci* 537:736–745. <https://doi.org/10.1016/j.jcis.2018.11.045>
  35. Wang X, Liu X, Xiao C, Zhao H, Zhang M, Zheng N (2020) Triethylenetetramine-modified hollow Fe<sub>3</sub>O<sub>4</sub>/SiO<sub>2</sub>/chitosan magnetic nanocomposites for removal of Cr(VI) ions with high adsorption capacity and rapid rate. *Microporous Mesoporous Mater* 297. <https://doi.org/10.1016/j.micromeso.2020.110041>
  36. Zheng Y, Cheng B, Fan J, Yu J, Ho W (2021) Review on nickel-based adsorption materials for Congo red. *J Hazard Mater* 403:123559. <https://doi.org/10.1016/j.jhazmat.2020.123559>
  37. Vijayakumar S, Nilavukkarasi M, Vidhya E, Punitha VN, Prathipkumar S (2022) Biogenesis of Heneicosane mediated ZnO Nanoparticles: characterization and Biological Efficiency. *Chem Afr* 13:1–7. <https://doi.org/10.1007/s42250-022-00509-y>
  38. Kolodziejczak-Radzimska A, Jesionowski T (2014) Zinc oxide: from synthesis to application: a review. *Mater (Basel)* 7(4):2833–2881. <https://doi.org/10.3390/ma7042833>
  39. Kamal T, Ul-Islam M, Khan SB, Asiri AM (2015) Adsorption and photocatalyst assisted dye removal and bactericidal performance of ZnO/chitosan coating layer. *Int J Biol Macromol* 81:584–590. <https://doi.org/10.1016/j.ijbiomac.2015.08.060>
  40. Sun L, Shao R, Tang L, Chen Z (2013) Synthesis of ZnFe<sub>2</sub>O<sub>4</sub>/ZnO nanocomposites immobilized on graphene with enhanced photocatalytic activity under solar light irradiation. *J Alloy Compd* 564:55–62. <https://doi.org/10.1016/j.jallcom.2013.02.147>
  41. Ghahramanifard F, Rouhollahi A, Fazlollahzadeh O (2018) Electrodeposition of Cu-doped p-type ZnO nanorods; effect of Cu doping on structural, optical and photoelectrocatalytic property of ZnO nanostructure. *Superlattices Microstruct* 114:1–14. <https://doi.org/10.1016/j.spmi.2017.07.019>
  42. Belkhaoui C, Mzabi N, Smaoui H, Daniel P (2019) Enhancing the structural, optical and electrical properties of ZnO nanoparticles through (Al + Mn) doping. *Results Phys* 12:1686–1696. <https://doi.org/10.1016/j.rinp.2019.01.085>
  43. Sharma M, Joshi M, Nigam S, Shree S, Avasthi DK, Adelung R (2019) ZnO tetrapods and activated carbon based hybrid composite: adsorbents for enhanced decontamination of hexavalent chromium from aqueous solution. *Chem Eng J* 358:540–551. <https://doi.org/10.1016/j.cej.2018.10.031>
  44. Sharma M, Joshi M, Nigam S, Avasthi DK, Adelung R, Srivastava SK (2019) Efficient oil removal from wastewater based on polymer coated superhydrophobic tetrapodal magnetic nanocomposite adsorbent. *Appl Mater Today* 17:130–141. <https://doi.org/10.1016/j.apmt.2019.07.007>
  45. Chowdhury A, Khan AA, Kumari S, Hussain S (2019) Superadsorbent Ni–Co–S/SDS nanocomposites for Ultrahigh removal of Cationic, Anionic Organic Dyes and toxic metal ions: kinetics, isotherm and adsorption mechanism. *ACS Sustain Chem Eng* 7(4):4165–4176. <https://doi.org/10.1021/acssuschemeng.8b05775>
  46. Lee B, Jeon D, Yoo WJ, Seo JK, Shin SH, Han K, Kim SG, Park J (2013) Fiber-optic pH sensor based on sol–gel film immobilized with neutral rRed. *Opt Rev* 20:209–213. <https://doi.org/10.1007/s10043-013-0037-y>
  47. Budnyak TM, Pylypchuk IV, Tertykh VA, Yanovska ES, Koldynska D (2015) Synthesis and adsorption properties of chitosan-silica nanocomposite prepared by sol–gel method. *Nanoscale Res Lett* 10:87. <https://doi.org/10.1186/s11671-014-0722-1>
  48. Wu Z, Sun G, Jin W, Hou H, Wang S, Xin Q (2008) Nafion® and nano-size TiO<sub>2</sub>–SO<sub>4</sub><sup>2-</sup> – solid superacid composite membrane for direct methanol fuel cell. *J Membrane Sci* 313(1–2):336–343. <https://doi.org/10.1016/j.memsci.2008.01.027>
  49. Zhou H, Chen Y, Fan H, Shi H, Luo Z, Shi B (2008) Water vapor permeability of the polyurethane/TiO<sub>2</sub> nanohybrid membrane with temperature sensitivity. *J Appl Polym Sci* 109(5):3002–3007. <https://doi.org/10.1002/app.28427>
  50. Khayet M, Villaluenga JPG, Valentin JL, López-Manchado MA, Mengual JI, Seoane B (2005) Filled poly(2,6-dimethyl-1,4-phenylene oxide) dense membranes by silica and silane modified silica nanoparticles: characterization and application in pervaporation. *Polymer* 46(23):9881–9891. <https://doi.org/10.1016/j.polymer.2005.07.081>
  51. Jian P, Yahui H, Yang W, Linlin L (2006) Preparation of polysulfone–Fe<sub>3</sub>O<sub>4</sub> composite ultrafiltration membrane and its behavior in magnetic field. *J Membrane Sci* 284(1–2):9–16. <https://doi.org/10.1016/j.memsci.2006.07.052>
  52. Shen J, Xi J, Zhu W, Chen L, Qiu X (2006) A nanocomposite proton exchange membrane based on PVDF, poly(2-acrylamido-2-methyl propylene sulfonic acid), and nano-Al<sub>2</sub>O<sub>3</sub> for direct methanol fuel cells. *J Power Sources* 159(2):894–899. <https://doi.org/10.1016/j.jpowsour.2005.11.070>
  53. Bottino A, Capannelli G, Comite A (2002) Preparation and characterization of novel porous PVDF-ZrO<sub>2</sub> composite membranes. *Desalination* 146:35–40. [https://doi.org/10.1016/s0011-9164\(02\)00469-1](https://doi.org/10.1016/s0011-9164(02)00469-1)
  54. Marzuki M, Rusdi NM, Zain MZM, Izaki M (2021) Multi-staged sol–gel synthesis of mg doped ZnO/CuO core-shell heterojunction nanocomposite: dopant induced and interface growth



- response. *J Solgel Sci Technol* 100(3):388–403. <https://doi.org/10.1007/s10971-021-05679-8>
55. Hassan TB, Salih SM (2021) Synthesis of ZnO-CdO nanocomposite by sol–gel for NO<sub>2</sub> gas sensing. *Mater Today Proc* 42:2320–5. <https://doi.org/10.1016/j.matpr.2020.12.322>
  56. Baoum A, Amin MS (2022) Amended photocatalytic degradation of tetracycline applying sol–gel assembled CuO@rGO nanocomposite under visible light. *Opt Mater* 123. <https://doi.org/10.1016/j.optmat.2021.111956>
  57. Wang Y-t, Zhang X-t, Xu J-b, Shen Y, Wang C-a, Li F-w (2021) Fabrication and characterization of Al–CuO nanocomposites prepared by sol–gel method. *Def Technol* 17(4):1307–1312. <https://doi.org/10.1016/j.dt.2020.06.029>
  58. Wang J, Zhou Q, Song D, Qi B, Zhang Y, Shao Y (2015) Chitosan–silica composite aerogels: preparation, characterization and Congo red adsorption. *J Solgel Sci Technol* 76(3):501–509. <https://doi.org/10.1007/s10971-015-3800-7>
  59. Wu J-B, Zang S-Y, Yi Y-L (2013) Sol–gel derived ion imprinted thiocyanato-functionalized silica gel as selective adsorbent of cadmium(II). *J Solgel Sci Technol* 66(3):434–442. <https://doi.org/10.1007/s10971-013-3029-2>
  60. Viltužnik B, Lobnik A, Košak A (2014) The removal of hg(II) ions from aqueous solutions by using thiol-functionalized cobalt ferrite magnetic nanoparticles. *J Solgel Sci Technol* 74(1):199–207. <https://doi.org/10.1007/s10971-014-3596-x>
  61. Bhowmicka T, Ghoshb A, Nage S, Majumdera SB (2022) Sensitive and selective CO<sub>2</sub> gas sensor based on CuO/ZnO bilayer thin- film architecture. *J Alloys Compd* 903:163871
  62. Liu J, Chen Y, Zhang H (2021) Study of highly sensitive formaldehyde sensors based on ZnO/CuO. Heterostructure via the sol–gel Method *Sensors* 21:4685
  63. Cao C, Yu L, Xie Y, Wei W, Jin H (2022) Hydrogen production by supercritical water gasification of lignin over CuO-ZnO catalyst synthesized with different methods. *Int J Hydrog Energy* 47:8716–8728
  64. Modwi A, Ghanem MA, Al-Mayouf AM, Houas A (2018) Lowering energy band gap and enhancing photocatalytic properties of Cu/ZnO composite decorated by transition metals. *J Mol Struct* 1173:1–6
  65. Truong TT, Pham TT, Truong TTT, Pham TD (2022) Synthesis, characterization of novel ZnO/CuO nanoparticles, and the applications in photocatalytic performance for rhodamine B dye degradation. *Environ Sci Pollut Res* 29:22576–22588
  66. Katiyar A, Kumar N, Shukla RK, Srivastava A (2020) Influence of alkali hydroxides on synthesis, physico-chemical and photoluminescence properties of zinc oxide nanoparticles. *Mater Today Proc* 1(29):885–9. <https://doi.org/10.1016/j.matpr.2020.05.112>
  67. Suwannahong K, Wongcharee S, Kreetachart T, Sirilamduan C, Rioyo J, Wongphat A (2021) Evaluation of the Microsoft Excel Solver Spreadsheet-Based program for nonlinear expressions of Adsorption Isotherm Models onto magnetic. *Nanosorbent Appl Sci* 11:7432. <https://doi.org/10.3390/app11167432>
  68. Batool F, Akbar J, Iqbal S, Noreen S, Bukhari SN (2018) Study of isothermal, kinetic, and thermodynamic parameters for adsorption of cadmium: an overview of linear and nonlinear approach and error analysis. *Bioinorg Chem Appl* 2018. <https://doi.org/10.1155/2018/3463724>
  69. Chan LS, Cheung WH, Allen SJ, McKay G (2012) Error analysis of adsorption isotherm models for acid dyes onto bamboo derived activated carbon. *Chin J Chem Eng* 20(3):535–542
  70. Hsieh S-H, Ting J-M (2018) Characterization and photocatalytic performance of ternary Cu-doped ZnO/Graphene materials. *Appl Surf Sci* 427:465–75. <https://doi.org/10.1016/j.apsusc.2017.06.176>
  71. Chakrabarty S, Mahmud MA, Ara MH, Bhattacharjee S (2021) Development of a platform for removal of Iron (III) ions from aqueous solution using CuO nanoparticles. *J Water Environ Nanotechnol* 6(1):41–48. <https://doi.org/10.22090/jwent.2021.01.004>
  72. Chitra K, Annadurai G (2013) Antimicrobial activity of wet chemically engineered spherical shaped ZnO nanoparticles on food borne pathogen. *Int food Res J* 20(1):59–64
  73. Karthik K, Jaya NV, Kanagaraj M, Arumugam S (2011) Temperature-dependent magnetic anomalies of CuO nanoparticles. *Solid State Commun* 151(7):564–568. <https://doi.org/10.1016/j.ssc.2011.01.008>
  74. Kaur M, Kumari S, Sharma P (2020) Removal of pb (II) from aqueous solution using nanoadsorbent of Oryza sativa husk: Isotherm, kinetic and thermodynamic studies. *Biotechnol Rep* 25:e00410. <https://doi.org/10.1016/j.btre.2019.e00410>
  75. Moyo M, Chikazaza L, Nyamunda BC, Guyo U (2013) Adsorption batch studies on the removal of pb(II) using maize tassel based activated carbon. *J Chem* 508934:8. <https://doi.org/10.1155/2013/508934>
  76. Doyurum S, Celik A (2006) Pb(II) and cd(II) removal from aqueous solutions by olive cake. *J Hazard Mater* 138:22–28. <https://doi.org/10.1016/j.jhazmat.2006.03.071>
  77. Tunali S, Akar T, Ozcan AS, Kiran I, Ozcan A (2006) Equilibrium and kinetics of biosorption of lead (II) from aqueous solutions by *Cephalosporium aphidicola*. *Sep Purif Technol* 47(3):105–112. <https://doi.org/10.1016/j.seppur.2005.06.009>
  78. Srinivasa RJ, Kesava RC, Prabhakar G (2013) Optimization of biosorption performance of Casuarina leaf powder for the removal of lead using central composite design. *J Environ Anal Toxicol* 3:166. <https://doi.org/10.4172/2161-0525.1000166>
  79. El-Latif MMA, Ibrahim AM, Showman MS, Hamide RRA (2013) Alumina/Iron oxide nano composite for cadmium ions removal from aqueous solutions. *Int J Nonferrous Metall* 2:47–62. <https://doi.org/10.4236/ijnm.2013.22007>
  80. Martini T, Anandita EP (2019) Activation and characterization of andisol soil and fly ash composite in adsorption of lead (II) metal ion. *J Phys Conf Ser* 1295(1):012012. <https://doi.org/10.1088/1742-6596/1295/1/012012>
  81. Ifijen IH, Itua AB, Maliki M, Ize-Iyamu CO, Omorogbe SO, Aigbodion AI, Ikhuoria EU (2020) The removal of nickel and lead ions from aqueous solutions using green synthesized silica microparticles. *Heliyon* 6(9):e04907. <https://doi.org/10.1016/j.heliyon.2020.e04907>
  82. Meena AK, Mishra GK, Rai PK, Rajagopal C, Nagar PN (2005) Removal of heavy metal ions from aqueous solutions using carbon aerogel as an adsorbent. *J Hazard Mater* 122:161–170. <https://doi.org/10.1016/j.jhazmat.2005.03.024>
  83. Dargahi GH, Darvishi P, Karami A, Hasan SH, Poormohammadi A, Behzadnia A (2016) An investigation and comparison of removing heavy metals (lead and chromium) from aqueous solutions using magnesium oxide nanoparticles. *Pol J Environ Stud* 25:p–557. <https://doi.org/10.15244/pjoes/60281>
  84. Das, Mondal NK (2011) Calcareous soil as a new adsorbent to remove lead from aqueous solution: equilibrium, kinetic and thermodynamic study. *Univers J Environ Res Technol* 1(4):515–530
  85. Langmuir I (1916) The constitution and fundamental properties of solids and liquids. Part 1. Solids. *Am Chem Soc* 38(11):2221–2295. <https://doi.org/10.1021/ja02268a002>
  86. Freundlich HMF (1906) Über die Adsorption in Losungen. *Z für Phys Chemie* 57(1):385–470. <https://doi.org/10.1515/zphc-1907-5723>



87. Yang C (1998) Statistical mechanical study on the freundlich isotherm equation. *J Colloid Interface Sci* 208(2):379–387. <https://doi.org/10.1006/jcis.1998.5843>
88. Ragadhita R, Nandiyanto AB (2021) How to calculate adsorption isotherms of particles using two-parameter monolayer adsorption models and equations. *Indonesian J Sci Technol* 6(1):205–234
89. Lagregren S (1898) About the theory of so-called adsorption of soluble substances. *Kungliga Svenska Vetenskapsakademiens Handlingar* 24:1–39
90. Ho YS, McKay G (1999) Pseudo-second-order model for sorption processes. *Process Biochem* 34:451–465. [https://doi.org/10.1016/s0032-9592\(98\)00112-5](https://doi.org/10.1016/s0032-9592(98)00112-5)
91. He Y, Wu P, Xiao W et al (2019) Efficient removal of pb(II) from aqueous solution by a novel ion imprinted magnetic biosorbent: adsorption kinetics and mechanisms. *PLoS ONE* 14:1–17. <https://doi.org/10.1371/journal.pone.0213377>
92. Zhou K, Yang ZG, Liu YC, Kong X (2015) Kinetics and equilibrium studies on biosorption of pb(II) from aqueous solution by a novel biosorbent: *cyclosorus interruptus*. *J Environ Chem Eng* 3:2219–2228. <https://doi.org/10.1016/j.jece.2015.08.002>
93. Nassar NN (2010) Rapid removal and recovery of pb(II) from wastewater by magnetic nano-adsorbents. *J Hazard Mater* 184(1):538–546. <https://doi.org/10.1016/j.jhazmat.2010.08.069>
94. Dargahi A, Golestanifar H, Darvishi P et al (2016) An investigation and comparison of removing heavy metals (lead and chromium) from aqueous solutions using magnesium oxide nanoparticles. *Pol J Environ Stud* 25(2):557–562. <https://doi.org/10.15244/pjoes/60281>
95. Venkatesham V, Madhu GM, Satyanarayana SV, Preetham HS (2013) Adsorption of lead on Gel Combustion Derived Nano ZnO. *Procedia Eng* 51:308–313. <https://doi.org/10.1016/j.proeng.2013.01.041>
96. Fan HT, Wu JB, Fan XL, Zhang DS, Su ZJ, Yan F, Sun T (2012) Removal of cadmium (II) and lead (II) from aqueous solution using sulfur-functionalized silica prepared by hydrothermal-assisted grafting method. *Chem Eng J* 198:355–363. <https://doi.org/10.1016/j.cej.2012.05.109>
97. Mahdavi S, Jalali M, Afkhami A (2012) Removal of heavy metals from aqueous solutions using Fe<sub>3</sub>O<sub>4</sub>, ZnO, and CuO nanoparticles. *J Nanopart Res* 14:1–18. <https://doi.org/10.1007/s11051-012-0846-0>
98. Tabesh S, Davar F, Loghman-Estarki MR (2018) Preparation of -Al<sub>2</sub>O<sub>3</sub> nanoparticles using modified sol-gel Method and its use for the adsorption of lead and cadmium ions. *J Alloys Compd* 730:441–449. <https://doi.org/10.1016/j.jallcom.2017.09.246>
99. Tirtom VN, Dincer A, Becerik S, Aydemir T, Celik A (2012) Removal of lead (II) ions from aqueous solution by using crosslinked chitosan-clay beads. *Desalin Water Treat* 39:76–82. <https://doi.org/10.1080/19443994.2012.669161>
100. Kocabas O, Yurum Y (2013) Synthesis and characterization of anatase nano-adsorbent and application in removal of lead, copper and arsenic from water. *Chem Eng J* 225:625–635. <https://doi.org/10.1016/j.cej.2013.03.106>
101. Mostafa NG, Yunnus AF, Elawwad A (2022) Adsorption of Pb (II) from water onto ZnO, TiO<sub>2</sub>, and Al<sub>2</sub>O<sub>3</sub>: process study, adsorption behaviour, and thermodynamics. *Adsorp Sci Technol* 2022
102. Karaçetin G, Sivrikaya S, Imamoğlu M (2014) Adsorption of methylene blue from aqueous solutions by activated carbon prepared from hazelnut husk using zinc chloride. *J Anal Appl Pyrol* 110:270–276
103. Dutta SK, Amin MK, Ahmed J, Elias M, Mahiuddin M (2022) Removal of toxic methyl orange by a cost-free and eco-friendly adsorbent: mechanism, phytotoxicity, thermodynamics, and kinetics. *S Afr J Chem Eng* 40:195–208
104. Saxena M, Kushwaha JP, Kulshreshtha S, Kaur G (2022) Singh N (2022) Doxycycline adsorptive interaction with mesoporous MCM-41: kinetic and isotherm modelling with thermodynamics. *Chem Afr* 19(1–4):1055–1068. <https://doi.org/10.1007/s42250-022-00365-w>

**Publisher's Note** Springer Nature remains neutral with regard to jurisdictional claims in published maps and institutional affiliations.

Springer Nature or its licensor (e.g. a society or other partner) holds exclusive rights to this article under a publishing agreement with the author(s) or other rightsholder(s); author self-archiving of the accepted manuscript version of this article is solely governed by the terms of such publishing agreement and applicable law.